electronics

MDPI

Article

A Wideband Polarization-Reconfigurable Antenna Based on Fusion of TM_{10} and Transformed-TM_{20} Mode

Xianjing Yuan †, Siyuan Zheng †, Binyun Yan * and Weixing Sheng

School of Electronic and Optical Engineering, Nanjing University of Science and Technology, Nanjing 210094, China; yuanxianjing@njust.edu.cn (X.Y.); zhengsiyuan@njust.edu.cn (S.Z.); shengwx@njust.edu.cn (W.S.)

* Correspondence: yanby@njust.edu.cn

† These authors contributed equally to this work.

Abstract: A wideband polarization-reconfigurable microstrip antenna based on a mode-fusion mechanism is proposed. This simple antenna structure consists of a rectangular radiation patch and a ground, both with crossed slots. The slots crossing the ground are connected by eight PIN diodes and four capacitors such that two orthogonal linear-polarization radiation modes can be realized. The radiation patch is slotted such that a transformed TM_{20} mode is excited, realizing broadside radiation that the traditional TM_{20} mode is unable to. With fusion of the fundamental TM_{10} mode and the transformed-TM_{20} (T-TM_{20}) mode, a wide bandwidth of 30.1% is achieved in two reconfigurable polarizations. The measured results agree well with the simulation results. The total efficiency of the proposed antenna is more than 80.0% over the bandwidth.

Keywords: reconfigurable antennas; broadband antennas; mode fusion

check for updates

Citation: Yuan, X.; Zheng, S.; Yan, B.; Sheng, W. A Wideband Polarization-Reconfigurable Antenna Based on Fusion of TM_{10} and Transformed-TM_{20} Mode. *Electronics* **2024**, *13*, 3760. https://doi.org/10.3390/electronics13183760

Academic Editor: Djuradj Budimir

Received: 7 August 2024
Revised: 8 September 2024
Accepted: 16 September 2024
Published: 22 September 2024

1. Introduction

Polarization-reconfigurable antennas [1] are gaining popularity due to their capability of dynamic polarization adjustment according to system requirements. In recent years, various techniques have been investigated to realize antenna polarization reconfigurability, mainly including mechanical-servo systems [2], RF switches [3], and tunable material control methods [4].

These techniques are generally based on the mechanisms of reconfiguring the radiator shape [4,5], the feeding network [6,7], and loaded metasurface structures [8,9]. Twelve PIN diodes are placed on the radiator; by selectively turning these diodes on or off, six LPs can be generated [5]. In addition to radiators, another technique for achieving polarization diversity is reconfiguring the feeding network. A PIN-controlled feeding network is designed to change the amplitude and phase of the two linear polarized components by switching between the three polarizations of horizontal linear polarization (LP), vertical LP, and circular polarization (CP) [7]. Moreover, metasurface structures have been applied to change antenna polarization. A slot antenna and PIN diode-controlled single-substrate reconfigurable polarizer can be combined to achieve right-hand circular polarization (RHCP) or left-hand circular polarization (LHCP) with a bandwidth of 1.6% [8]. These reconfigurable states cannot share a wide band, as the polarization is reconfigured by the change in the electric current on the radiator. As a result, a mismatch appears at the antenna port depending on whether the radiator, the feed network, or the radiation field is modulated.

To achieve a wider bandwidth, aperture-coupled feeding is an effective technique [10]. This technique is also used to avoid a soldering connection between feed circuits and radiating elements, which can interfere with the patch radiation. The aperture-coupled patch antenna can achieve an impedance bandwidth of 23%; however, the liquid–metal control requires a bulky mechanical servo system consisting of syringes or electrochemically controlled capillarity (ECC) [4]. Another way to realize a wide band is to adopt a reconfigurable feed network that combines complex power divides and phase shifters.

In [6], the phase difference between the feed ports was reconfigured by the wideband feed network, with the overlapping bandwidth at each polarization reaching 34%. However, the structure of the feed network is complicated and requires many voltage points to be controlled independently. Creating and collaboratively utilizing multiple resonances significantly enhances the bandwidth of polarization-reconfigurable antennas [11].

In addition, multimodal coupling theory can be used to provide multiple resonances [12]. The antenna in [13] not only integrates four operating modes (TM_{10}, TM_{30}, TM_{12}, and TM_{32} modes), it also doubles the operating bandwidth. More importantly, this design uses the interactions of various modes of the patch antenna to correct the radiation patterns. Similarly, by asymmetrically loading a stub on one radiating edge of the patch and cutting a rectangular slot offset from the other one, the current distributions of the TM20 and TM30 modes are perturbed, resulting in broadside radiation for all of the first three modes of a single patch [14]. A compact wideband dipole antenna based on odd and even mode fusion was presented in [15]. By moving the feed point and adding decoupling branches in addition to the basic odd mode, the even mode of the dipole is excited and its bandwidth is expanded. Fusion of the TM_{10} and TM_{20} modes is often used to improve antenna performance [16]. Such antennas mainly utilize mode fusion to broaden the beam width. When TM_{10} mode is excited on only the right sub-patch and TM_{20} mode is excited on the whole patch, the two modes have the same resonant frequency; in this way, the radiation patterns of the TM_{10} and TM_{20} modes become fused, broadening the beam width of the radiation pattern. Similarly, the mode-fusion technique for enhancing bandwidth can be applied to polarization-reconfigurable antennas.

In this article, a wideband polarization-reconfigurable microstrip antenna based on the mode fusion principle is proposed. The TM_{10} and TM_{20} modes of the square microstrip patch are analyzed based on the cavity model theory. By etching gaps in the radiating patch and the slot-coupled microstrip feed, it is possible to prevent the broadside radiation pattern of TM_{20} mode from being null, which provides the antenna with a broader operation bandwidth. By controlling the PINs in the ground orthogonal slots, the proposed antenna allows for switching between horizontal and vertical polarizations in a wide bandwidth from 2.15 GHz to 2.94 GHz. Low cross-polarization gain can be maintained in the operating band. This design avoids the need for a complex reconfigurable matching network or complicated DC biasing circuit.

2. Antenna Structure and Reconfigurable Principle

2.1. Geometry of the Antenna

The structure of the proposed antenna is shown in Figure 1. It mainly consists of two substrate layers and a metal cavity. A square radiation patch with two etched orthogonal gaps is printed on the top of Sub1. The upper surface of Sub2 consists of the ground along divided into four pieces (labeled 1–4 in clockwise order). The 50 Ω microstrip feed line on the bottom of Sub2 is fed by an SMA coaxial cable. Both substrates are Rogers R04003C substrates with a thickness of 1.5 mm ($\varepsilon_r = 3.55$, $\tan\delta = 0.0027$); the height of the air layer between the two substrates is 10 mm. The presence of the air gap not only increases the impedance bandwidth of the antenna but also improves the radiation efficiency and gain [17]. The metal support structure that makes up the metal cavity is split into four parts to avoid DC contact. The inner dimension of the metal cavity is 110 mm × 110 mm × 10 mm.

The metal cavity improves the impedance matching of the antenna and promotes the fusion of the two resonance points. This metal cavity consists of four L-shaped aluminum blocks, which are also used for fixing the upper and lower dielectric substrates. The presence of the metal cavity allows enough space for the placement of the PIN diodes and capacitors. The four openings are designed to prevent the ground, which is divided into four pieces, from being electrically connected, meaning that the bias circuit can easily apply a voltage to the ends of the PIN diodes to make them conductive. In addition, the metal cavity binds the electromagnetic wave radiation, further improving the antenna's gain.

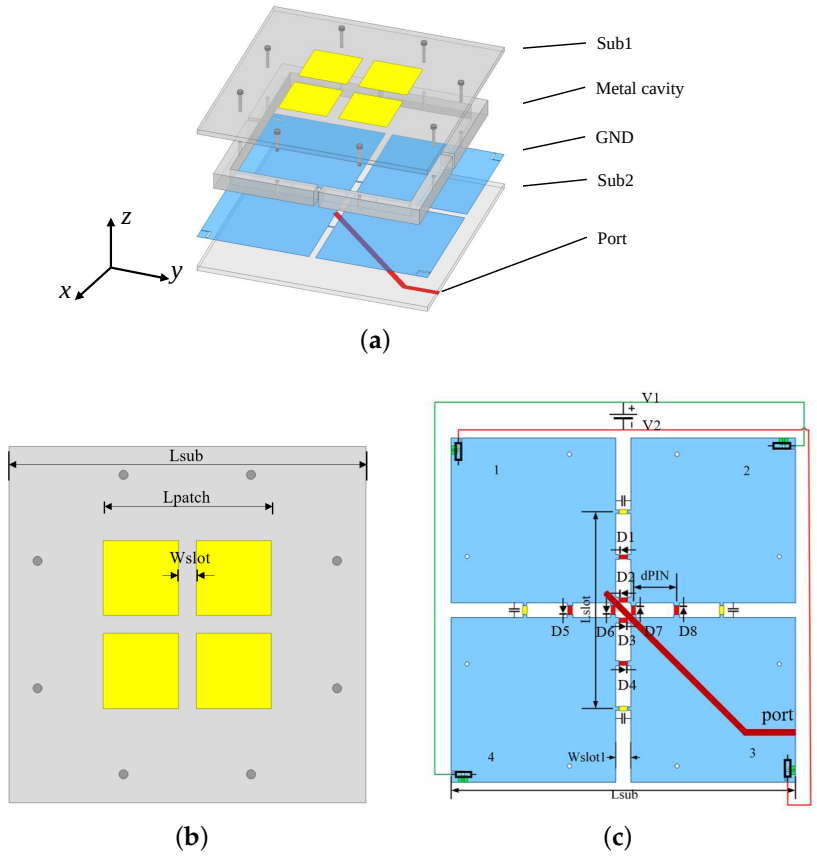

Figure 1. Geometrical configuration of the proposed antenna: (**a**) 3D view, (**b**) Sub1 view, and (**c**) Sub2 view.

The orthogonal feed slots divide the ground into four parts. Due to the cracked metal cavity, separate voltages can be loaded into the four parts. Two PIN diodes are placed in each slot between two close parts. The arrangement of the PIN diodes (D1–D8), capacitors, and resistors is shown in Figure 1c. The geometrical dimensions of the overall antenna structure and surface mount device (SMD) component values were optimized using the HFSS simulator. The final design values are included in Table 1.

Table 1. Optimized dimensions of the proposed antenna.

Parameter	Lsub	Lpatch	Wslot	dPIN	Wslot1	Lslot
Units (mm)	140	66	10	13	4	70

2.2. Transformed TM_{20} Model and Mode Fusion Principle

For a conventional square patch, TM_{10} and TM_{30} modes both have a broadside radiation pattern, while TM_{20} mode radiates a null pattern on the broad side. Because the resonant frequencies of two adjacent odd modes are usually far apart from each other, the transformed TM_{20} mode (even-order mode) is taken into consideration. The equivalent magnetic currents and electric field distributions of the TM_{10} and TM_{20} modes of operation are shown in Figure 2.

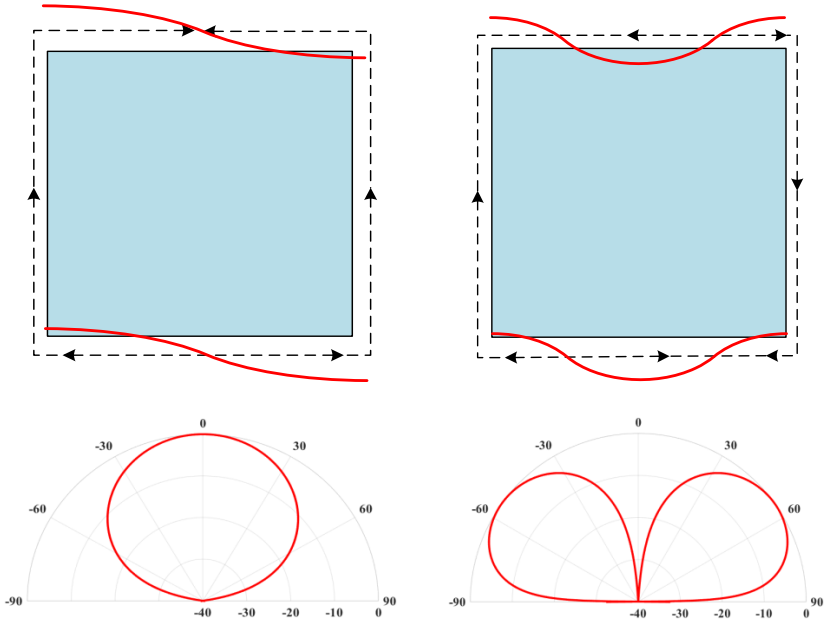

Figure 2. The equivalent magnetic currents (black dashed lines with arrow) and *E*-plane electric field distributions (red lines) of (**a**) the traditional TM_{10} mode and (**b**) TM_{20} mode with the typical radiation patterns.

According to [18], the radiation pattern of a magnetic current source in the *xoz* plane ($\varphi = 0°$) can be calculated using Equation (1):

$$F(\theta) = \frac{\sin(kH\sin\theta)}{\sin\theta}\cos\theta \tag{1}$$

where k is the propagation constant in free space, H is the spacing between the magnetic current source and the ground (to simplify the arithmetic, we take $kH = 1$) and θ is the deflection angle from the positive z-axis. Then, the radiation patterns of the rectangular patches under ideal conditions can be calculate by introducing the array factor. Figure 2a,b shows the calculation results for a rectangular patch working in the traditional TM_{10} mode and TM_{20} mode obtained from Equations (2) and (3).

$$F_1(\theta) = \frac{\sin(kH\sin\theta)}{\sin\theta}\cos\theta\left(1 + e^{jkl\sin\theta}\right) \tag{2}$$

$$F_2(\theta) = \frac{\sin(kH\sin\theta)}{\sin\theta}\cos\theta\left(1 - e^{jkl\sin\theta}\right) \tag{3}$$

In TM_{10} mode, the equivalent magnetic currents on opposite sides of the patch flow in the same direction, forming a stable broadside direction. However, in TM_{20} mode the equivalent magnetic currents on both sides are reversed, leading to a zero point in the broadside radiation.

The center gap on the radiator changes the electric field distribution in the cavity of the antenna, as shown in Figure 3.

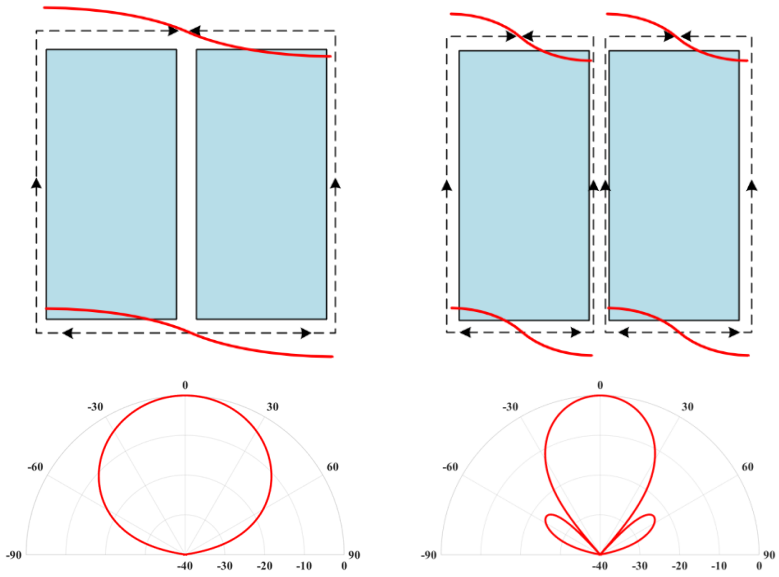

(**a**) (**b**)

Figure 3. The equivalent magnetic currents (black dashed lines with arrow) and *E*-plane electric field distributions (red lines) of (**a**) TM10 mode and (**b**) T-TM20 mode with the improved radiation patterns.

Due to the magnitude of the electric field being 0 at the center, the gap barely affects operation in TM_{10} mode. However, the gap is located at the electric field's maximum in TM_{20} mode, which breaks the continuity of the electric field distribution in this mode. Due to the presence of strong coupling currents on the gap, the direction of the electric field on both sides of the gap is abruptly changed. The gap also flips the direction of the equivalent magnetic current on both sides of the patch. In Figure 4, the transformed TM_{20} mode (T-TM_{20} mode) produces four equivalent magnetic currents in the same direction, creating a stable broadside pattern which can be calculated using Equation (4).

$$F_3(\theta) = \frac{\sin(kH\sin\theta)}{\sin\theta}\cos\theta\left(1 + e^{jk\frac{(l-d)}{2}\sin\theta} + e^{jk\frac{(l+d)}{2}\sin\theta} + e^{jkl\sin\theta}\right) \tag{4}$$

In addition, the gap facilitates the fusion of the two modes in terms of resonant frequency. Due to the gap, the current path of the TM_{10} mode of the antenna is reduced, moving the operating frequency of this mode towards higher frequencies. Meanwhile, because of the edge effect, the gap provides an additional current path that shifts the operating frequency of the T-TM_{20} mode towards lower frequencies. According to the cavity mode theory of a typical microstrip antenna [19], the frequency calculation formulas for the two resonant points of the antenna are inferred as follows:

$$f_1 = \frac{c}{2\left(W_{patch} - W_{slot} + 2\Delta w\right)\sqrt{\varepsilon_e}} \tag{5}$$

$$f_2 = \frac{c}{2\left(\left(W_{patch} - W_{slot}\right)/2 + 2\Delta w\right)\sqrt{\varepsilon_e}} \tag{6}$$

where W_{patch} is the width of the patch, W_{slot} is the width of the slit, and Δw is the extending width due to the effect of the fringing field. By coupling these two neighboring resonant modes, the antenna can achieve a wider -10 dB impedance bandwidth. In addition, the gap behaves as the capacitive loading, which also contributes to bandwidth enhancement.

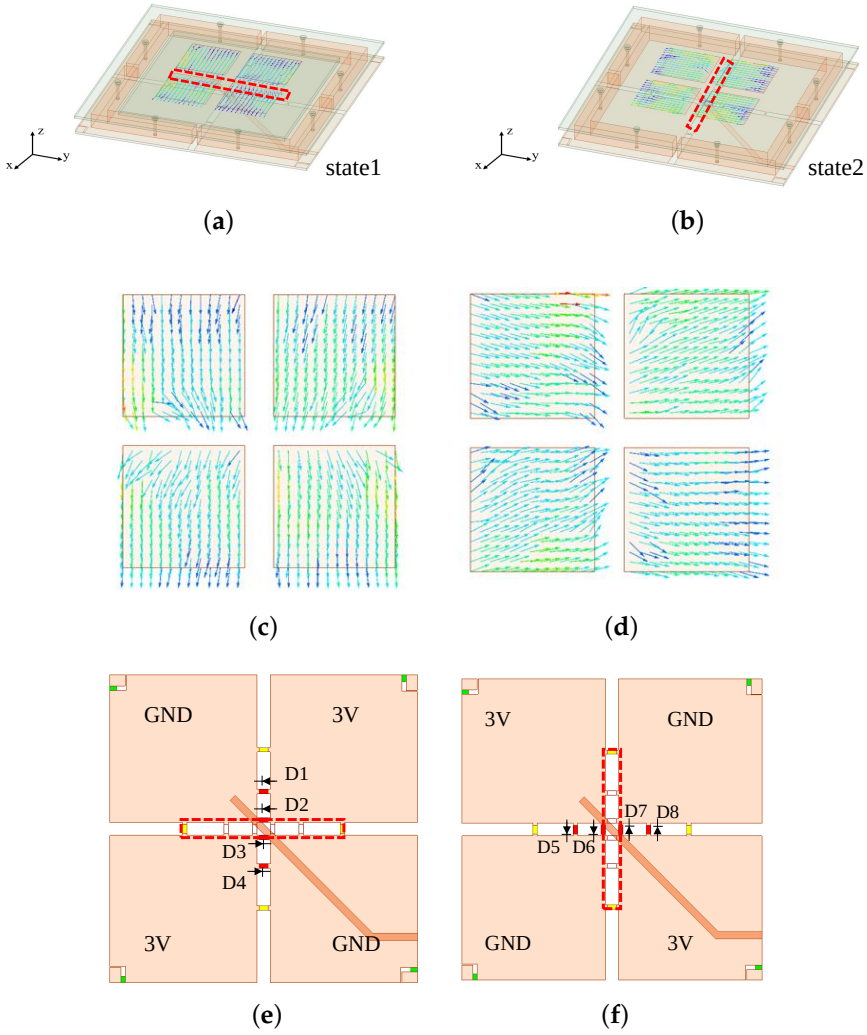

Figure 4. Current distribution of the antenna: (**a**) state1 and (**b**) state2. Top view of the current distribution on the antenna patch in (**c**) state1 and (**d**) state2. PIN diodes on/off on antenna ground in (**e**) state1 and (**f**) state2.

2.3. Realization of Polarization Reconfigurability

The design of the polarization-reconfigurable antenna is developed based on the multimodal coupling wideband antenna shown in Section 2.2. On the basis of the mode-fusion principle, orthogonal gaps are etched on the patch, realizing a combination of the TM_{10}/TM_{01} and T-TM_{20}/T-TM_{02} modes. When TM_{10} mode and T-TM_{20} mode are excited with the corresponding gap, the other unrelated gap barely influences the operation, as it is parallel to the current direction of the two modes.

The proposed antenna introduces an aperture-coupled feeding method to excite two working modes at the same time. In order to obtain polarization-reconfigurable characteristics, two switchable cross slots are etched on the ground to achieve different polarization states. The ground is divided into four parts by cross slots, and eight PIN diodes (D1–D8) are placed in the counterclockwise direction connect the ground separated by the slots to each other. By applying different voltages to both ends of the ground in order to control the switching of the PIN diodes, the ground becomes equivalent to a rectangular slot in the center of a whole ground with different directions of switching, allowing the direction of the antenna aperture coupling to be changed to achieve switching of the polarization. Due to the excellent DC isolation and RF conduction characteristics of large capacitors, four 100 pF capacitors are placed in the ground slot to control the length of the slot and four

50 Ω resistors are placed between the DC source and the diodes to protect the PIN diodes from breakdowns.

To simplify the control circuit, the diodes are arranged in the orientation shown in Figure 1; two diagonal sections of the ground are connected by the green and red wires, respectively (Number 1 and 3 are connected, 2 and 4 are connected). The voltages of the two parts are noted as V1 and V2. Polarization switching is achieved by applying different voltages to the connecting wires in Figure 1 to shield different slots. When diodes D1–4 are on and diodes D5–8 are off, the result is X-polarization; otherwise, the result is Y-polarization. The relationship between the polarization and the states of the eight PIN diodes is tabulated in Table 2.

Table 2. Polarization state control via eight diodes.

State	V1	V2	D1–D4	D5–D8	Polarization
1	+3 V	0 V	ON	OFF	X-polarization
2	0 V	+3 V	OFF	ON	Y-polarization

The current distribution of the antenna's radiating patch and the on/off states of the PIN diodes on the antenna ground for both polarization states are shown in Figure 4. For state 1, as shown in Figure 4e, diodes D1–D4 are on and diodes D5–D8 are off at this voltage, which is equivalent to etching a slot (framed by the red dashed line) along the Y-axis direction in the center of the ground. As a result, the antenna is fed through the aperture coupling, which excites a current distributed along the X-axis direction on the radiating patch, achieving X-axis direction line polarization, as seen in Figure 4c. Correspondingly, for state 2, diodes D5–D8 are on and diodes D1–D4 are off at this voltage, which is equivalent to etching a slot along the X-axis direction in the center of the ground; due to the symmetry of the antenna structure, linear polarization is achieved in the Y-axis direction, as seen in Figure 4d,f.

The electric field distributions of the substrate around the radiation patch are shown in Figure 5. The electric field is strongest at the red arrow. It can be seen that the distribution of electric field vectors in the antenna cavity at two resonant frequencies is in perfect agreement with the theoretical situation deduced above in Figure 3. At the low-frequency resonance point, the electric field distribution near the patch has only one electric field period, which corresponds to the electric field distribution of the TM_{10} mode shown in Figure 3a, whereas at the high-frequency resonance point, the electric field distribution near the patch has two independent electric field periods, which corresponds to the transformed TM_{20} mode and matches with the electric field distribution curve in Figure 3b.

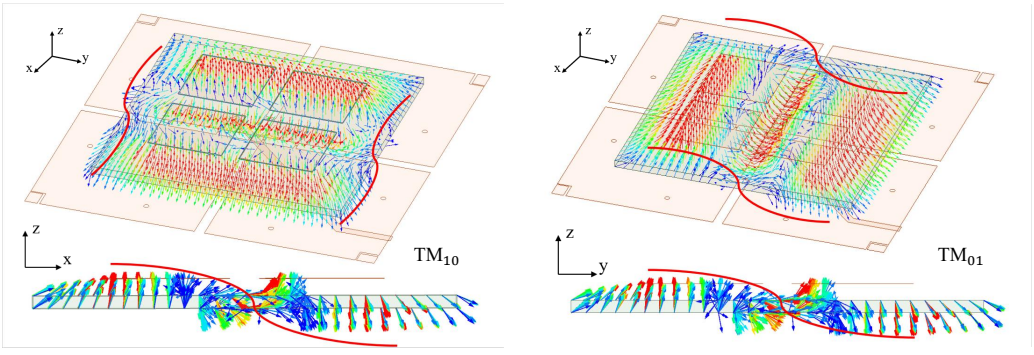

(**a**) (**b**)

Figure 5. *Cont.*

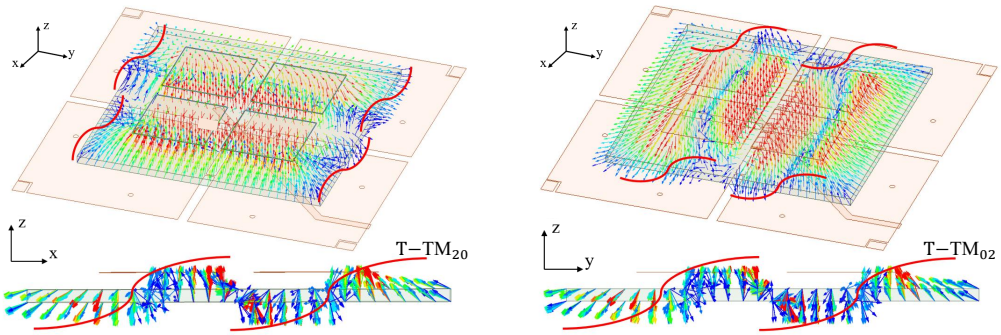

(**c**) (**d**)

Figure 5. Vector electric field distributions of the substrate around the radiation patch: (**a**) 2.4 GHz and (**c**) 2.8 GHz in state1; (**b**) 2.4 GHz and (**d**) 2.8 GHz in state2.

2.4. Parametric Analysis

The size of the metal cavity in the antenna has a large impact on its impedance matching. The dimensions of the cavity are analyzed in Figure 6a. When the metal cavity is larger, the antenna's return loss is larger and the impedance matching is better. Considering the size of the antenna, and leaving space for the bias circuit to be designed, the final side length of the metal cavity was chosen as 110 mm. The outer wall of the metal cavity is slightly smaller than the size of the ground, which makes it easier to solder RF connectors and DC source wires at the edge of the ground while at the same time shielding the induced current on the wire from the antenna's radiation.

Low cross-polarization is another consideration for polarization-reconfigurable antennas. The position of the two PIN diodes in this design is an important variable in controlling the cross-polarization. Two adjacent sections of the ground are connected by two PIN diodes at a distance of dPIN. Figure 6b explores the effect of different distances of the two diodes on the antenna's cross-polarization performance. When dPIN = 13 mm, the antenna achieves a cross-polarization of −20 dB. This is due to the fact that at this point the PIN diodes can be positioned to best shield the slot and reduce the individual radiation from the short slot to the upper small patch; therefore, the improvement in cross polarization can be obtained more noticeably in the higher frequency bands.

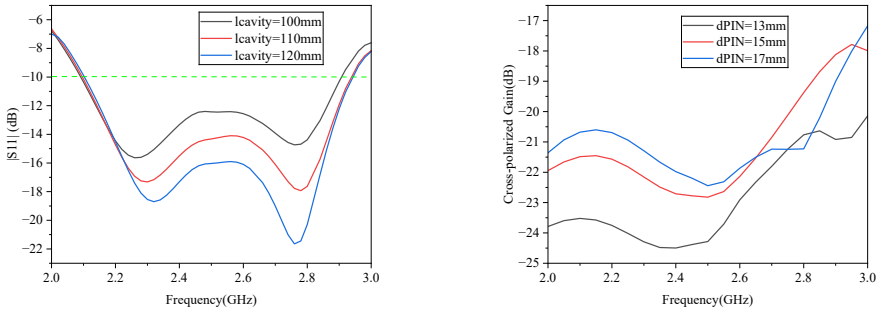

(**a**) (**b**)

Figure 6. Parametric analysis: (**a**) frequency response of |S11| as a function of the side length of the metal cavity and (**b**) frequency response of the antenna's cross-polarization gain with dPIN at 2.4 GHz.

3. Simulation and Measurement Results

Modeling and investigation of the proposed antenna were carried out in the HFSS simulator, a full-wave electromagnetic (EM) simulation software. In the simulations, the ON–OFF state of the PIN diodes (MADP-000907-14020) were modeled according to the equivalent circuit model (see Figure 7) provided by the datasheet.

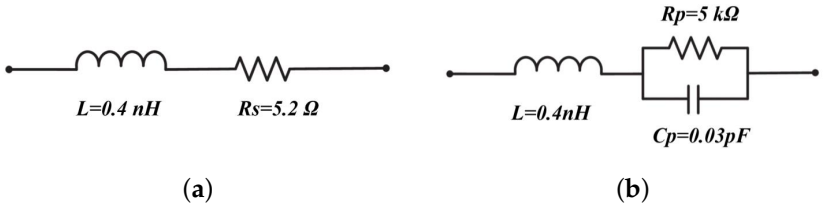

Figure 7. Equivalent circuit models for MADP-000907-14020: (**a**) ON-state and (**b**) OFF-state.

To verify the rationality of the antenna design, the proposed polarization-reconfigurable antenna was fabricated and experimentally validated. Sub1 and Sub2 were processed according to the standard printed circuit board fabrication process, consisting of a metal cavity made of four aluminum metal frames. All structures were hinged together by metal studs. The prototype of the proposed antenna is shown in Figure 8.

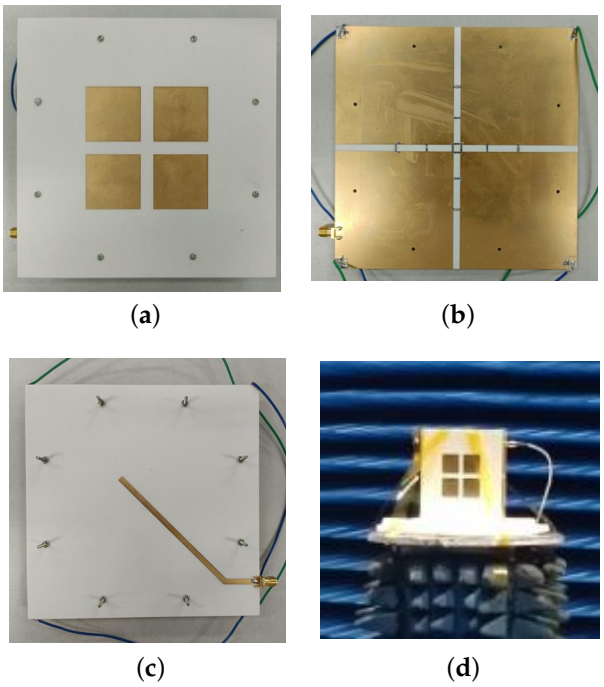

Figure 8. Prototype of proposed polarization-reconfigurable antenna: (**a**) top view of Sub1, (**b**) top view of Sub2, (**c**) bottom view of sub2, and (**d**) setup for measuring radiation.

In the antenna impedance measurements, bias voltage was provided by a DC source. During the test, the current of the DC source was 0.04 A at 3 V, which proves that the four PIN diodes were all in normal operating condition. The simulated and measured |S11| of the proposed antenna are depicted in Figure 9a. The measurements show good agreement with the simulation results. It can be seen that the |S11| curves of the two states are highly overlapped due to the symmetrical structure of the antenna. Meanwhile, the proposed antenna exhibits dual-resonant behavior in the two resonant frequencies of 2.4 GHz and 2.8 GHz, which correspond to the TM_{10}/TM_{01} and T-TM_{20}/T-TM_{02} modes. By coupling these two neighboring resonant modes, the proposed antenna can achieve a wider −10 dB impedance bandwidth of 2.15–2.94 GHz (30.1%).

Figure 10 shows the normalized radiating patterns of the proposed antenna on the E- and H-planes at the two resonant frequencies in different states. The E-plane patterns at the two resonant frequencies are in agreement with the theory of analysis, as shown in Figure 3. Figure 9b reports the realized gain across the operating bandwidth of the antenna for the main polarization and cross-polarization. The curves are similar to the simulation results. The gain range of the proposed antenna is 6.5–9.5 dBi. In the simulation,

the antenna has at least −19.5 dB cross polarization in both states and maintains −15 dB in measurement. Figure 11 demonstrates the efficiency of the antenna, which is higher than 80% in the operating band.

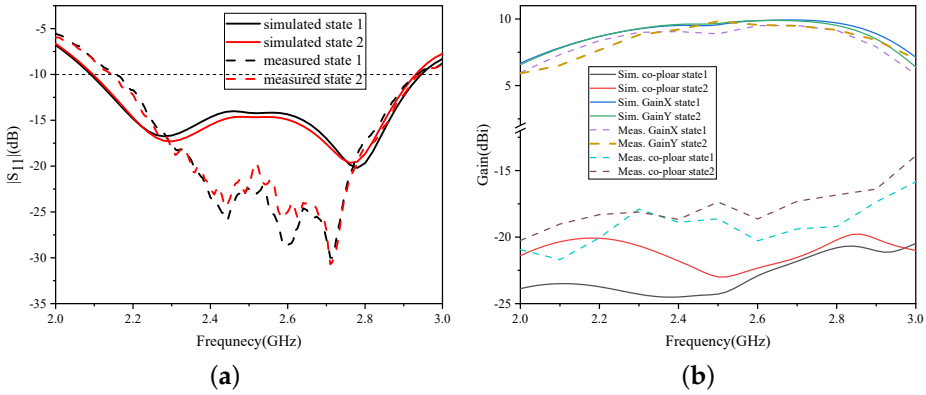

Figure 9. (**a**) Simulated and measured input reflection coefficients and (**b**) gain and co-gain frequency response curves for states 1 and 2.

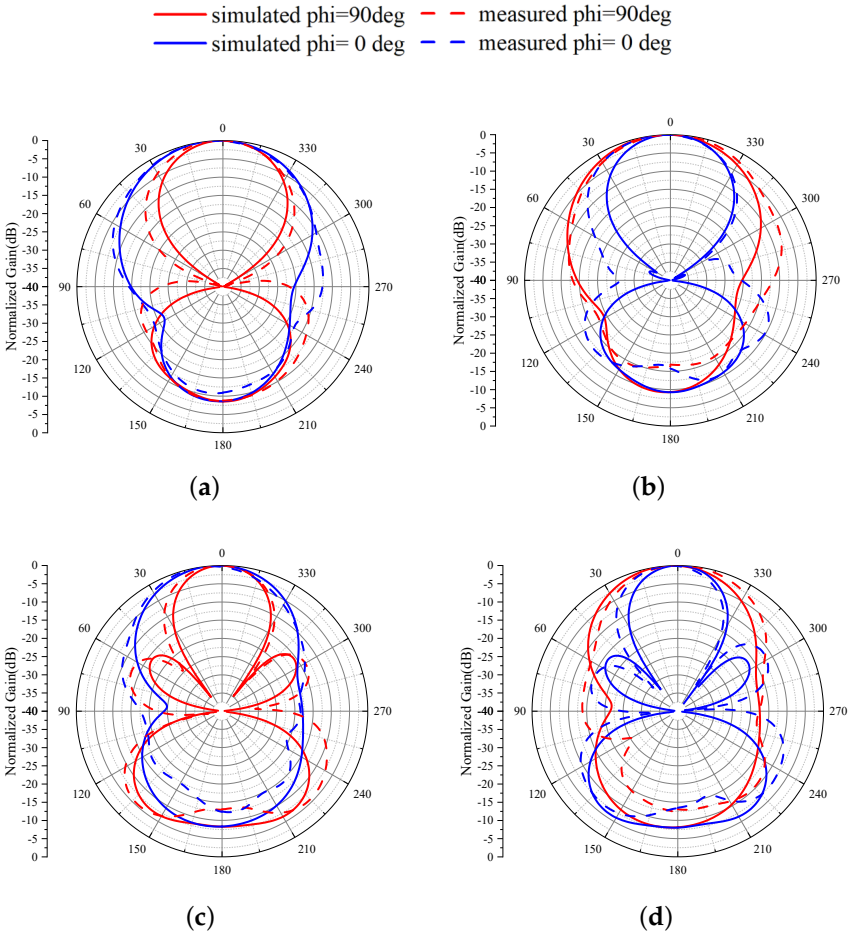

Figure 10. Radiation patterns of: (**a**) state 1 and (**b**) state 2 at 2.4 GHz; (**c**) state 1 and (**d**) state 2 at 2.8 GHz.

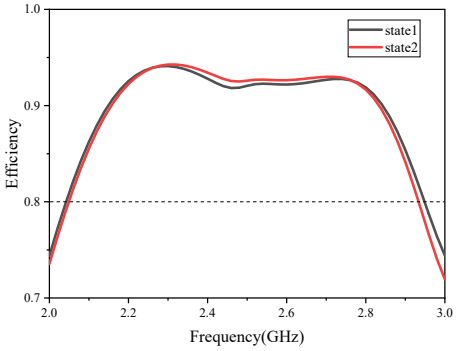

Figure 11. Efficiency frequency response curve.

Finally, Table 3 shows comparisons with several previous polarization-reconfigurable antennas. It can be seen that the proposed antenna provides a good balance of overall size and functionality.

Table 3. Comparison with previous polarization-reconfigurable antennas.

Ref.	Overlapped Bandwidth	No. of Polarization	Feeding Network	Methodology	Number of Control Voltages	Size at	Peak Gain (dBi or dBic)	Radiation Efficiency
[3]	1.18%	3	No	2 PIN Diodes	3	$0.5 \times 0.5 \times 0.016$	2.55	N/A
[4]	23.20%	3	No	Liquid Metal	N/A *	$0.82 \times 0.82 \times 0.08$	7.24	90%
[6]	8%	6	Yes	6 PIN Diodes	10	$0.625 \times 0.625 \times 0.16$	7.07	N/A
[7]	16%	3	Yes	8 PIN Diodes	9	$0.65 \times 0.65 \times 0.067$	4.38	N/A
[8]	1.60%	2	No	32 PIN Diodes	2	$1.01 \times 1.01 \times 0.09$	9.6	70%
[9]	33.30%	3	No	Mechanical rotation	N/A	$2.53 \times 2.53 \times 0.1$	16.5	N/A
[11]	27.60%	3	No	4 PIN Diodes	5	$0.4 \times 0.4 \times 0.04$	6.39	86%
This work	30.10%	2	Yes	8 PIN Diodes	2	$1.19 \times 1.19 \times 0.11$	9.5	80%

* N/A means Not Applicable.

4. Conclusions

A wideband polarization-reconfigurable microstrip antenna based on mode fusion has been proposed. Two resonance points are achieved by multiplexing the TM_{10} and transformed TM_{20} (T-TM_{20}) modes. By controlling the PIN diodes placed in the slots etched on the ground, which minimized the influences of the DC biasing circuits, the orthogonal line polarizations are able to switch with a wide impedance bandwidth of about 30.1% in the fraction. The proposed antenna has a simple control bias circuit without complex feeding networks, and has good efficiency over the operating bandwidth. With its low cost, simple structure, and convenient switching method, this antenna represents a promising polarization-reconfigurable design.

Author Contributions: Conceptualization, X.Y. and S.Z.; methodology, X.Y. and S.Z.; validation, X.Y. and S.Z.; formal analysis, X.Y. and S.Z.; investigation, X.Y. and S.Z.; resources, W.S.; writing—original draft preparation, X.Y. and S.Z.; writing—review and editing, X.Y., B.Y. and W.S.; visualization, X.Y.; supervision, B.Y. and W.S.; project administration, B.Y. and W.S.; funding acquisition, B.Y. All authors have read and agreed to the published version of the manuscript.

Funding: This work was supported by the China Postdoctoral Science Foundation under Grant 2023M741703.

Data Availability Statement: All data are contained within the article.

Conflicts of Interest: The authors declare no conflicts of interest.

References

1. Yang, F.; Rahmat-Samii, Y. A reconfigurable patch antenna using switchable slots for circular polarization diversity. *IEEE Microw. Wirel. Compon. Lett.* **2002**, *12*, 96–98. [CrossRef]
2. Hwang, M.; Kim, G.; Kim, S.; Jeong, N.S. Origami-Inspired Radiation Pattern and Shape Reconfigurable Dipole Array Antenna at C-Band for CubeSat Applications. *IEEE Trans. Antennas Propag.* **2021**, *69*, 2697–2705. [CrossRef]

3. Nishamol, M.S.; Sarin, V.P.; Tony, D.; Aanandan, C.K.; Mohanan, P.; Vasudevan, K. An Electronically Reconfigurable Microstrip Antenna With Switchable Slots for Polarization Diversity. *IEEE Trans. Antennas Propag.* **2011**, *59*, 3424–3427. [CrossRef]
4. Wang, C.; Yeo, J.C.; Chu, H.; Lim, C.T.; Guo, Y.X. Design of a Reconfigurable Patch Antenna Using the Movement of Liquid Metal. *IEEE Antennas Wirel. Propag. Lett.* **2018**, *17*, 974–977. [CrossRef]
5. Chang, L.H.; Lai, W.C.; Cheng, J.C.; Hsue, C.W. A Symmetrical Reconfigurable Multipolarization Circular Patch Antenna. *IEEE Antennas Wirel. Propag. Lett.* **2014**, *13*, 87–90. [CrossRef]
6. Liu, B.; Qiu, J.; Wang, C. Polarization and Bandwidth Reconfigurable Rectangular Dielectric Resonator Antenna. In Proceedings of the 2020 IEEE International Symposium on Antennas and Propagation and North American Radio Science Meeting, Montreal, QC, Canada, 5–10 July 2020; pp. 167–168. [CrossRef]
7. Li, W.; Wang, Y.M.; Hei, Y.; Li, B.; Shi, X. A Compact Low-Profile Reconfigurable Metasurface Antenna With Polarization and Pattern Diversities. *IEEE Antennas Wirel. Propag. Lett.* **2021**, *20*, 1170–1174. [CrossRef]
8. Li, W.; Gao, S.; Cai, Y.; Luo, Q.; Sobhy, M.; Wei, G.; Xu, J.; Li, J.; Wu, C.; Cheng, Z. Polarization-Reconfigurable Circularly Polarized Planar Antenna Using Switchable Polarizer. *IEEE Trans. Antennas Propag.* **2017**, *65*, 4470–4477. [CrossRef]
9. Ni, C.; Chen, M.S.; Zhang, Z.X.; Wu, X.L. Design of Frequency-and Polarization-Reconfigurable Antenna Based on the Polarization Conversion Metasurface. *IEEE Antennas Wirel. Propag. Lett.* **2018**, *17*, 78–81. [CrossRef]
10. Targonski, S.; Pozar, D. Design of wideband circularly polarized aperture-coupled microstrip antennas. *IEEE Trans. Antennas Propag.* **1993**, *41*, 214–220. [CrossRef]
11. Li, M.; Zhang, Z.; Tang, M.C.; Zhu, L.; Liu, N.W. Bandwidth Enhancement and Size Reduction of a Low-Profile Polarization-Reconfigurable Antenna by Utilizing Multiple Resonances. *IEEE Trans. Antennas Propag.* **2022**, *70*, 1517–1522. [CrossRef]
12. Boyuan, M.; Pan, J.; Huang, S.; Yang, D.; Guo, Y. Wide-Beam Dielectric Resonator Antennas Based on the Fusion of Higher-Order Modes. *IEEE Trans. Antennas Propag.* **2021**, *69*, 8866–8871. [CrossRef]
13. Feng, S.; Zhang, L.; Weng, Z.; Jiao, Y.C. A Wideband Differential-Fed Microstrip Patch Antenna Based on Quad-Mode Resonance With Radiation Patterns Correction. *IEEE Trans. Antennas Propag.* **2023**, *71*, 5404–5409. [CrossRef]
14. Tan, Q.; Chen, F.C. Triband Circularly Polarized Antenna Using a Single Patch. *IEEE Antennas Wirel. Propag. Lett.* **2020**, *19*, 2013–2017. [CrossRef]
15. Huang, H.; Li, B.; Li, X.; Liu, Y. A Wideband Dipole Based on Odd and Even Mode Fusion. *IEEE Antennas Wirel. Propag. Lett.* **2024**, *23*, 783–787. [CrossRef]
16. Guan, L.; Cheng, Y.; Feng, J.; Liao, C. A novel planar wide-angle scanning phased array under operation of TM10 and TM20 modes. *Microw. Opt. Technol. Lett.* **2020**, *63*, 944–951. [CrossRef]
17. Yang, H.Y.D.; Alexopoulos, N.G.; Yablonovitch, E. Photonic band-gap materials for high-gain printed circuit antennas. *IEEE Trans. Antennas Propag.* **2002**, *45*, 185–187. [CrossRef]
18. Kraus, J.D.; Marhefka, R.J. *Antennas for All Applications*, 3rd ed.; McGraw-Hill: New York, NY, USA, 2003.
19. Balanis, C.A. *Antenna Theory: Analysis and Design*, 3rd ed.; Wiley-Interscience: Hoboken, NJ, USA, 1982.